Hindawi
International Journal of Antennas and Propagation
Volume 2022, Article ID 9002700, 11 pages
https://doi.org/10.1155/2022/9002700

Research Article

Compact Broadband Circularly Polarized CPW-Fed Antenna with Characteristic Mode Analysis

Wei Xu, Jingchang Nan, and Mingming Gao

School of Electronic and Information Engineering, Liaoning Technical University, Huludao 125100, China

Correspondence should be addressed to Wei Xu; xuwei@lntu.edu.cn

Received 20 November 2021; Revised 16 December 2021; Accepted 23 December 2021; Published 10 January 2022

Academic Editor: Trushit Upadhyaya

A compact circularly polarized (CP) antenna is proposed for low-profile and wideband operation based on characteristic mode analysis (CMA). A ring patch with a gap and two arc-shaped metallic stubs as the radiator is analyzed and optimized by CMA to figure out the orthogonal modes and operating frequency band for potential good axial ratio (AR) performance. The studies of these CP modes provide a physical insight into the property of broadband circular polarization. Such an in-depth understanding paves the way for the proposal of novel CP antenna with separation between the design of radiator and feeding network. A 50-Ω coplanar waveguide (CPW) is introduced and placed appropriately to excite the desired modes based on the information from CMA, which employs two asymmetric ground planes to improve the performance in terms of AR and impedance matching. The antenna with a compact size of $0.71\lambda_0 \times 0.76\lambda_0 \times 0.038\lambda_0$ (λ_0 is the free-space wavelength at the center frequency of the 3-dB AR bandwidth) is fabricated and measured for validation. The realized gain varies from 1.6 to 3.1 dBic over the operating bandwidth characterized by the measured 10-dB impedance bandwidth of 83.8% (3.98–9.72 GHz) and 3-dB AR bandwidth of 70.3% (4.59–9.57 GHz), respectively.

1. Introduction

Circularly polarized (CP) microstrip antennas with the characteristics of reducing the multipath effects, polarization mismatches, and Faraday's rotation effects in the ionosphere [1, 2] are popular and attractive in modern wireless communication applications such as global positioning systems (GPS), synthetic aperture radar (SAR), radio frequency identification device (RFID) [3], etc. CP radiation can be regarded as the superposition of two orthogonal linearly polarized (LP) radiations with equal amplitude and in-phase quadrature [4]. Massive investigations indicate that the most important issue associated with CP antenna design is how to optimize the patch shapes and recognize the two linear polarized modes to be combined for circular polarization. Various geometries have been proposed to accomplish this task, including dual-feed technique and 90° hybrid [5], stacked patches [6], asymmetric patches [7], defective ground [8], slot structures [9], and array configurations [10].

However, these methods cannot ensure a final satisfactory solution in each design attempt through parameter sweeps or using automated optimization techniques [11, 12]. The success of the final design still largely depends on the intuition and experience. Lacking physical insight leads to various novel patch shapes rather difficult to transfer from one to another in the CP antenna designs [13]. The characteristic mode analysis (CMA) has been proved to be an excellent candidate for the analysis and design of antennas [14]. There is an eigenvalue or characteristic angle associated with each characteristic mode (CM) that can provide information about the mode resonance and radiating characteristics in absence of source. In fact, providing the physical insight into antenna radiation is the most fascinating part of CMA. Additionally, since CMs only depend on the shape and size of the conductor, antenna design can be performed in a controlled way [14].

CMA is proposed for the analysis of simple band-notched UWB planar monopole antennas in [15]. Paper [16] provides some design guidelines for the excitation of

broadband slotted planar antennas. In [17], CMA was first used to analyze metasurface, and multiple modes were excited simultaneously to achieve broadband. Feeding mechanism and placement for exciting specific mode(s) are discussed in [18]. Furthermore, [19] indicates how to place the antenna on the structure to excite specific mode(s). With the help of CMA, various CP antennas have been proposed with characteristics of performance enhancement [20], simple design procedure [21], wideband [22], stacked patch with multiple probes [23], and low profile and high directivity [24].

This paper proposes a novel CP antenna with compact size and broadband operation. Under the guidance of CMA, two arc-shaped metallic stubs are introduced into the ring patch with a gap as the radiator that has the potential to generate CP radiation over a broadband. By studying the current distribution and radiation pattern of the collection of CMs, the CPW-fed network consisting of a T-shaped strip, a tuning rectangle stub, and two asymmetric ground planes is designed and placed in the specified position according to the indication of CMA, which acts as a capacitive coupling element (CCE) to excite the desired modes. Finally, the full-wave simulation of the proposed antenna is carried out for final optimization. As a validation, an antenna is fabricated and measured to demonstrate a good performance of impedance matching and CP operation over a very wide bandwidth.

2. Characteristic Mode Analysis for CP Generation

The characteristic mode theory (CMT) was first proposed by Garbacz in 1968 and later refined by Harrington and Mautz in 1971. Characteristic modes are a set of surface currents and radiated fields that correspond to the eigenvectors of a particular weighted eigenvalue equation involving a generalized impedance matrix of the conductor [14]. According to CMA, the total current J on the perfect electric conductor (PEC) surface can be expressed as a linear superposition of characteristic mode currents J_n:

$$J = \sum_n \alpha_n J_n, \tag{1}$$

where J_n is the modal current for mode n and its weighting is determined by modal weighting coefficients (MWC), and α_n denotes the contribution of each mode to the total current. On the other hand, J can also be expressed as [25]

$$J = \sum_n \frac{V_n^i J_n}{1 + j\lambda_n}, \tag{2}$$

where V_n is called the modal excitation coefficient (MEC), which indicates the coupling between the excitation and the nth mode to determine whether the mode is excited by the antenna feed or incident field. λ_n is the eigenvalue corresponding to mode n. From equations (1) and (2), the MWC can be expressed:

$$\alpha_n = \frac{V_n^i}{1 + j\lambda_n}. \tag{3}$$

As λ_n is close to zero, the corresponding mode exhibits a resonance and radiates the most efficiently. For convenience of measuring the resonant frequency and potential contribution to the radiation of a mode, the modal significance (MS) is defined.

$$MS = \left| \frac{1}{1 + j\lambda_n} \right|. \tag{4}$$

The range of MS is 0 to 1. The mode resonates and radiates the most efficiently when $MS = 1$. Equations (3) and (4) denote that a desired mode to be excited needs two conditions, i.e., a large MS and a considerable MEC. The modal excitation depends on the properties of feeding such as the feeding mechanism, feeding position, etc. Hence a mode wants to dominate an antenna radiation at specific frequencies; it has to be fed properly.

Another important parameter is characteristic angle (CA), which models the phase angle between a modal current and its associated characteristic field, defined as follows:

$$CA = 180^\circ - \tan^{-1}(\lambda_n). \tag{5}$$

A mode resonates when $CA = 180^\circ$, which means the mode behaves as a good radiator in the condition of CA close to 180°, whereas modes with CA near 90° or 270° mainly store energy.

Based on the principle of CP generation, to form a CP wave by CMA acquires a pair of modes excited simultaneously with the same MS and CA difference of 90° and their modal currents are perpendicular to each other. Besides, the directivities of modal field at the same angle of interest can ensure a stable radiation pattern in far field.

3. CP Antenna Design with CMA

3.1. Existing Modes of the Ring Patch. In order to elucidate the principle of CP generation, CMA is performed on the ring patch to guide the reconstruction of the structure necessary to generate CP radiation. Outer radius of R_o and inner radius of R_i indicate the dimension of the ring, which is etched in the center of the 1.6-mm-thick FR-4 substrate ($\varepsilon_r = 4.4$). The geometrical configuration of the ring patch is shown in Figure 1(a). It should be noted that the radiation boundary is applied in all directions and dielectric layer with no ground is assumed to be loss-free for CMA.

The first six characteristic modes are calculated in terms of MS and CA at 3 GHz, as shown in Figure 2. The curves of modes 1 and 2 coincide perfectly, as well as modes 4 and 5. They resonate at 3.6 GHz and 6.7 GHz, respectively. In addition, mode 6 resonates at 9.6 GHz and mode 3 resonates at higher frequency. As portrayed in Figure 2(b), the CA difference between the overlapping modes is 0° meaning no contribution to the CP realization. It can be imagined that if the overlapping modes can be separated with a 90° CA difference, then the conditions for CP wave generation are

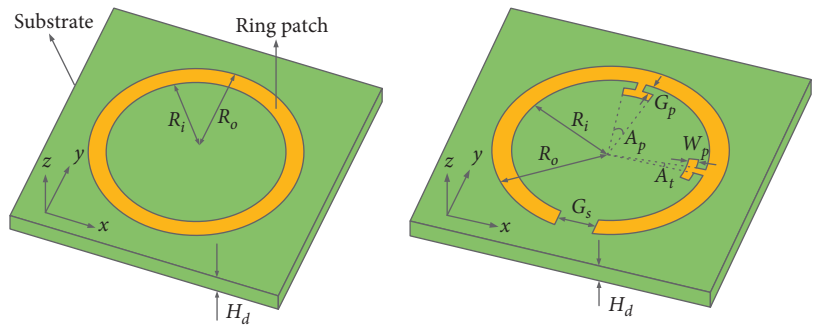

FIGURE 1: (a) Geometry of the ring patch: $R_o = 12$, $R_i = 10$, $H_d = 1.6$. (b) Geometry of the radiator: $R_o = 12$, $R_i = 10$, $H_d = 1.6$, $G_s = 4$, $A_p = 20^\circ$, $A_t = 5^\circ$, $G_p = 1$, $W_p = 1$. (Unit: mm).

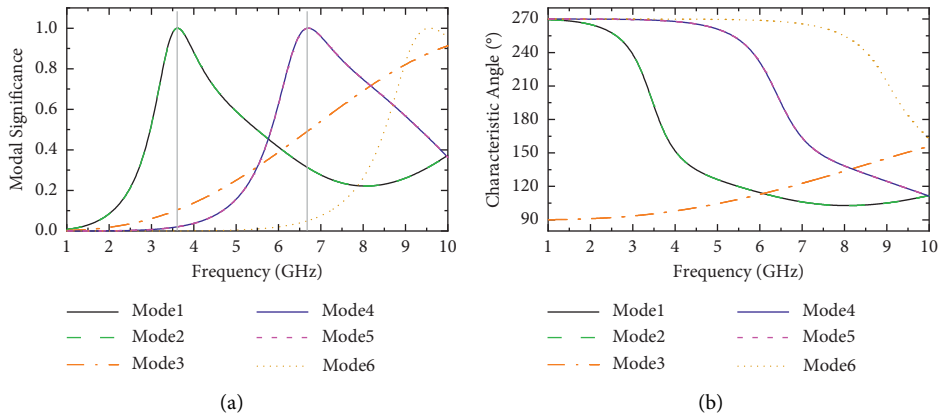

FIGURE 2: (a) Modal significance and (b) characteristic angle for the first six modes of the ring at 3 GHz.

achieved and the bandwidth is expanded. Generally, this can be accomplished by introducing perturbations.

3.2. Perturbations for CP Modes. To accommodate the conditions for generation of CP wave, i.e., the two operating modes have the same MS and 90° CA difference, a pair of perturbed stubs with the same dimension is proposed, and a section of the ring is cut off to form a gap of G_s, which leads to an asymmetric structure. As shown in Figure 1(b), the ring patch possesses the same dimension as the original one. The perturbed stub consists of two arc-shaped metallic strips with dimension of $A_p \times W_p$ and $A_t \times G_p$, where A_p and A_t are radians. The gap and two stubs are mounted along the ring, offset by 90° counterclockwise. The values of all the geometric parameters are shown in Figure 1's caption.

To reveal the CP operation of the proposed radiator, modal characteristics are investigated to provide current distribution and radiation pattern in far field in the absence of excitation. Furthermore, the geometry of the radiator has been optimized by means of the parametric analysis in CMA according to the requirements for generation of CP wave, which is not shown in the article for the sake of brevity.

Figure 3 portrays the first six characteristic modes over 1–10 GHz. With the exception of mode 2 resonating at around 1.6 GHz far away from the operating band, the remaining five modes form a collection of combined radiating modes that have the same MS of around 0.7. Meanwhile, their corresponding modal currents and radiation patterns are depicted in Figure 4 as well.

Mode 1 intersects mode 3 at 4.5 GHz, where the CA difference of 94° and orthogonal currents between the pair of degenerate modes indicated that the combination possesses the potential for CP radiation. Hence, the combination of modes 1 and 3 is named CP modes (CPM 1–3). A closer observation of the performance of the two modes in Figure 3 reveals that a single mode has low radiating efficiency at the frequency of CP modes intersection. This is because when the CA of a single mode deviates from resonance angle of 180°, the stored reactive energy increases while the radiating energy decreases. However, the CP modes can still yield 100% radiating efficiency due to compensation between the inductive energy of one mode and the capacitive energy of the other mode as they are excited at the same time.

As the frequency increases, the MS of mode 1 decreases while the MS of mode 4 increases and obtains the same MS with mode 3 at around 6 GHz. The perpendicular modal currents (J_3 and J_4) and the 102o CA difference make them have the potential to broaden CP operating band. Above 7 GHz, since the MS of modes 3 and 4 decay slowly after the

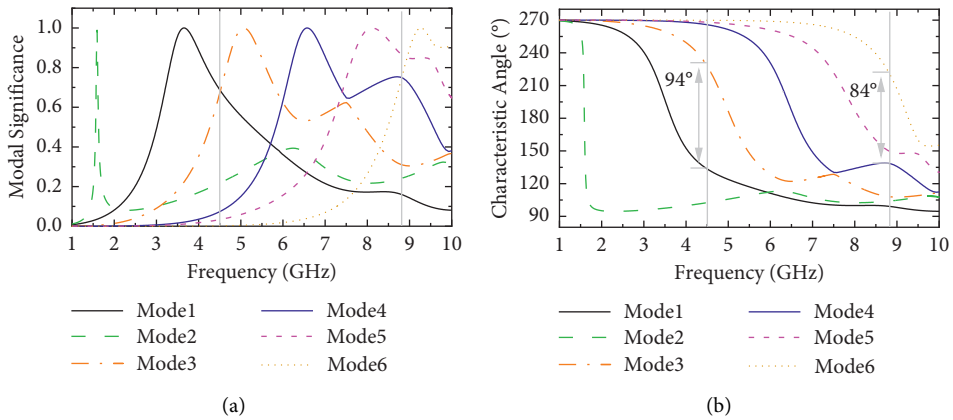

FIGURE 3: (a) Modal significance and (b) characteristic angle for the first six modes of radiator at 3 GHz.

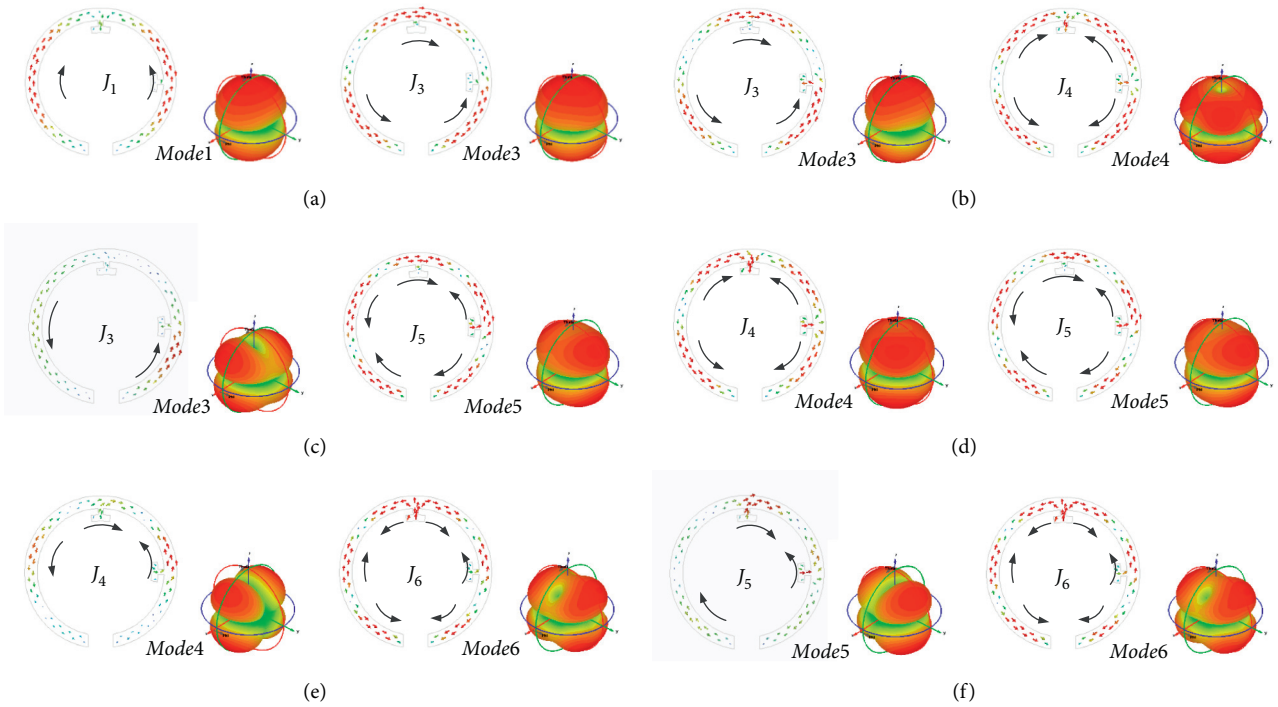

FIGURE 4: Modal currents and radiation patterns for the radiator of (a) Mode 1 and Mode 3 at 4.5 GHz. (b) Mode 3 and Mode 4 at 6 GHz. (c) Mode 3 and Mode 5 at 7.3 GHz. (d) Mode 4 and Mode 5 at 7.4 GHz. (e) Mode 4 and Mode 6 at 8.8 GHz. (f) Mode 5 and Mode 6 at 8.9 GHz.

intersection, four mode combinations (modes 3–5, modes 4–5, modes 4–6, and modes 5–6) have the same MS of around 0.7, which need to be further screened for CP modes according to the distribution of their corresponding modal currents. Clearly, the CPMs 3–5 and 4–6 feature CP potential due to their perpendicular modal currents and CA difference close to 90° at 7.3 GHz and 8.8 GHz, respectively. On the contrary, the modes 4–5 and modes 5–6 have little contribution to CP radiation due to their respective nonorthogonal currents.

In addition to modal currents, CMA also provides radiation patterns in far field for physical insight into antenna radiating characteristics. As portrayed in Figure 4, only modes J_1 and J_3 radiate at the boresight direction as the currents on the patch can be equivalent to one current in a single direction, whereas the other modes are characterized by cancellation of electric field in the far-field region at the boresight because their equivalent currents exhibit opposite directions with respect to the center of the patch. It should be noticed that although mode 3 still achieves boresight radiation pattern at around 6 GHz with an approximate 90° rotation for E-plane relative to that at 4.5 GHz, it generates a radiation null as the frequency rises to 7.3 GHz.

Through the above analysis, it can be concluded as follows: if the CP modes 1–3 are excited properly, a stable boresight radiation pattern for CP operation is achieved

around 4.5 GHz. Moreover, CPMs 3–4, 3–5, and 4–6 can be involved to further broaden CP bandwidth at the cost of radiation pattern stability. Thus, it can be reasonably understood that the total radiation pattern of the proposed antenna may tilt away from boresight direction at some frequencies. In a word, the radiator features wideband CP potential over 4.5–8.8 GHz in pursuit of bandwidth.

3.3. Determination of Feeding Placement. The diversity of CMs provides the possibility to excite the desired mode for designing antennas with different characteristics at certain frequency [13]. Taking advantage of the property of modal currents, it provides useful information to determine the feeding mechanism, structure, and optimal feeding position, which separates the design of antenna radiator from the feeding network.

To excite CP modes with the same magnitude, the excitation should be set at the minimum difference between the operating modal currents [26]. In general, either inductive or capacitive coupling mechanisms can be used to excite CM [16]. At the location of the source, the modes with intense currents can be excited effectively by inductive feeding, whereas capacitive coupling mechanism is suitable for exciting the modes with strong electric field. The current difference distributions for each pair of CP modes are plotted in Figure 5. The minimum difference between the operating modal currents appears at the gap in all four cases. Combined with the current distribution of each mode in Figure 4, capacitive coupling mechanism should be applied.

3.4. Geometry of the Proposed Antenna. Figure 6 shows the geometry of the proposed antenna, which is mounted on the same substrate with dimension of $W \times L$ as the radiator. To keep the antenna compact while providing enough space for the feed, the radiator is rotated 90° counterclockwise and printed on the back of the substrate. The center of the radiator is located at the horizontal midpoint of the substrate, and the vertical distance from the lower edge of the substrate is 18.7 mm. All the geometric parameters are completely consistent with the radiator.

To excite the modes of interest and enhance the impedance bandwidth, an improved coplanar waveguide (CPW) is employed as feeding structure etched on the other side of the substrate. A W_f width signal strip is located in the center of the coplanar ground planes with two identical gaps of width G_f. As depicted in Figure 6, the left-hand and right-hand ground planes have the same width of W_g horizontally but different lengths vertically, L_{gl} and L_{gr}, respectively. The asymmetric T-shape feedline in conjunction with rectangular tuning stub accounts for capacitive coupling excitation, which is composed of two strips with widths W_1 and W_2, respectively. The vertical strip passes a distance of L_1 from the signal strip to the horizontal strip. Starting from the midpoint of the upper edge of the vertical strip, the horizontal strip extends to the gap of the ring by a length of L_2 and is connected to a $L_3 \times W_3$ capacitive coupling stub, whereas the reverse one extends a length of L_p for adding some tuning parameters.

The |MWC| or $|\alpha_n|$ of the first six modes are calculated using the commercial software CST Studio Suite 2021 for validating the effectiveness of the proposed feeding network. Figure 7 shows the calculated $|\alpha_n|$ ($n = 1, 2, \ldots, 6$), which measures the contribution of each $\mathbf{J}_n$ to the total radiated power. A dominant mode has a large $|\alpha_n|$ at a frequency thus large MS and $|V_n|$ simultaneously and vice versa. As can be seen, the resonant frequencies of lower modes (Modes 1, 2, and 3) shift upper and higher modes (modes 4, 5, and 6) shift down under the influence of the feed network. These modes all have large |MWC| in their working frequency band, indicating that they are effectively excited by the feeding network. For example, modes 1 and 3 at around 4.5 GHz dominate the radiation at lower frequencies. The other modes are not well excited with tiny |MWC| so their contribution is negligible compared to the modes 1 and 3.

3.5. Parametric Analysis. The introduced CPW feed alters the modal currents leading to the change of the characteristic fields of the radiator to deteriorate circular polarization characteristics. In order to improve antenna performance in terms of AR bandwidth (ARBW) and impedance matching, some key parameters are analyzed by full-wave simulation with the same boundary setup as CMA. The results are shown in Figure 8.

As shown, the width of ground plane can affect the impedance matching in the lower frequency band while it has almost no effect on the resonant frequency in the other frequency band. The analysis of W_g shows that, by varying its value, the lower cut-off frequency is slightly affected while the upper cut-off frequency can be controlled in terms of both S11 and AR.

To improve the performance of AR and impedance matching, the left-hand side of the ground with different length from the right-hand side is employed. The effects of L_{gl} are found to have a great impact on the performance of the antenna as shown in Figure 8(b). The length of left-hand ground plane controls the impedance matching, which also tunes the lower frequency of 3-dB AR. It should be noted that the effect of L_{gl} on AR and impedance is nonmonotonic where the intermediate value can provide better performance.

The variations of L_1 have great effects on both of the impedance matching and CP operation depicted in Figure 8(c). In fact, the value of L_1 is related to the position of the CCE feed, which takes critical part in exciting the desired mode. The impedance and AR bandwidth improve as L_1 decreases, especially at the upper frequencies.

As a tuner, parameter L_p plays an important role in improving the characteristics of impedance and CP. In Figure 8(d), with the increase of L_p, the impedance matching is improved, and the bandwidth is significantly broadened as well. However, deviating too far from the median ($L_p = 3$ mm) leads to AR violating the 3-dB criterion.

In short, a broadband response in terms of the impedance and AR bandwidth can be achieved by the optimized geometric parameters of the proposed antenna shown in Figure 6.

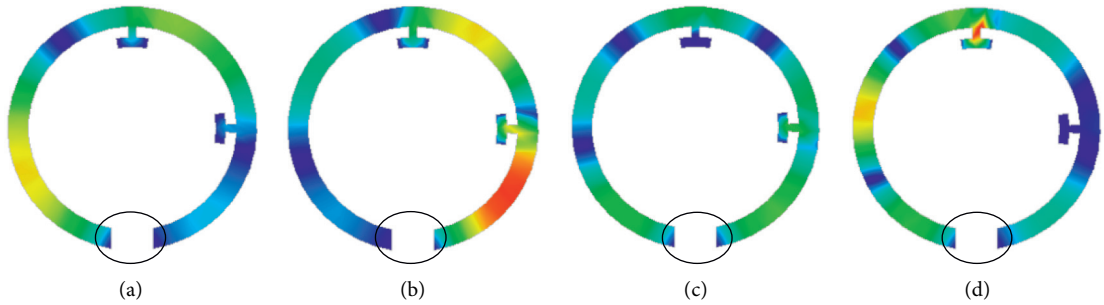

FIGURE 5: Current difference distribution between (a) J_1 and J_3 at 4.5 GHz, (b) J_3 and J_4 at 6 GHz, (c) J_3 and J_5 at 7.3 GHz, and (d) J_4 and J_6 at 8.8 GHz.

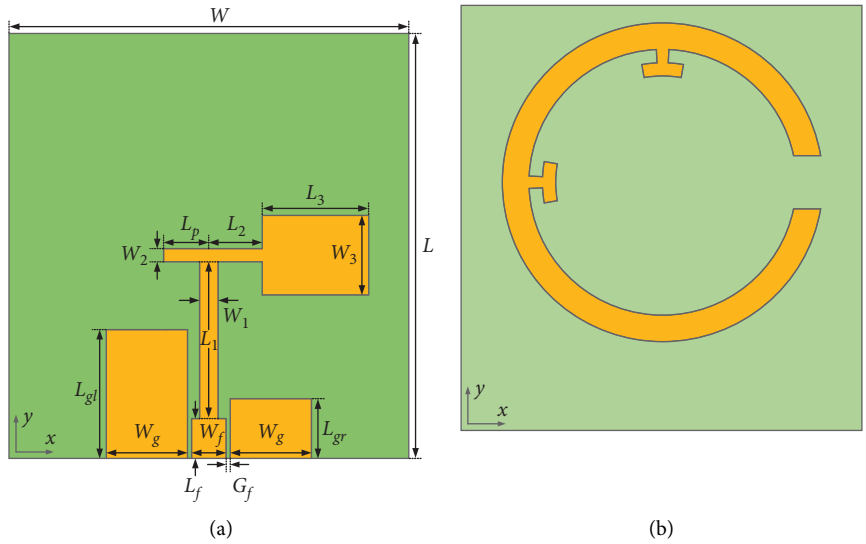

FIGURE 6: Geometrical of the proposed antenna: (a) Top view ($W = 30$, $L = 32$, $W_g = 6.1$, $L_{gl} = 9.7$, $L_{gr} = 4.5$, $W_f = 2.6$, $L_f = 3$, $G_f = 0.3$, $W_1 = 1.4$, $L_1 = 11.8$, $W_2 = 1$, $L_p = 3.4$, $L_2 = 4$, $W_3 = 6$, $L_3 = 8$ (Unit: mm). (b) Perspective view.

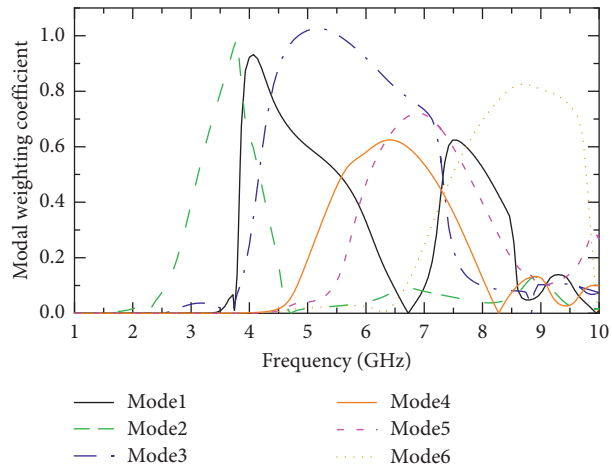

FIGURE 7: |MWC| for the first six modes excited by the CPW-fed network.

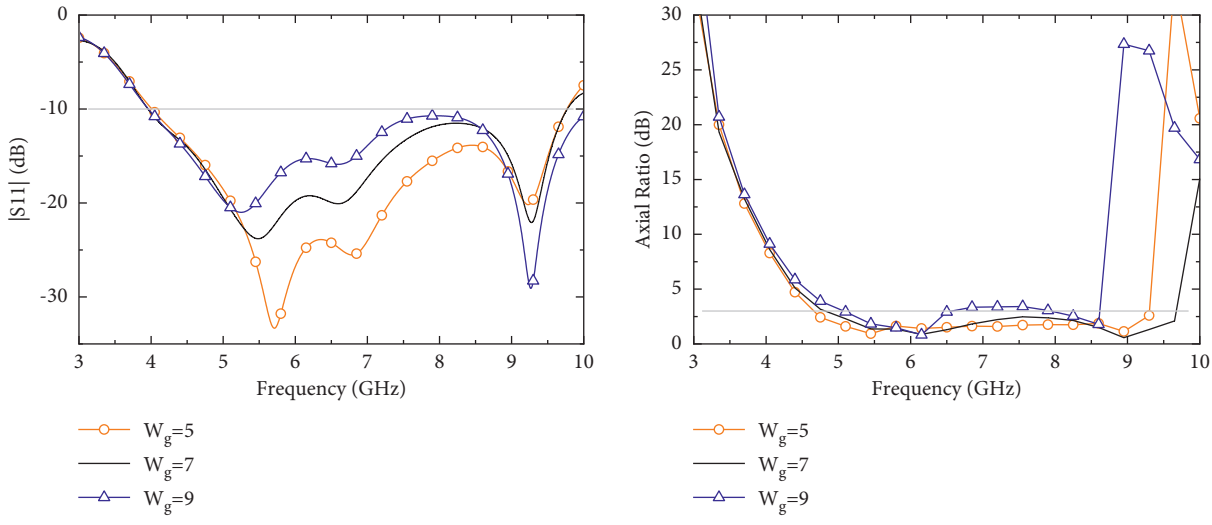

(a)

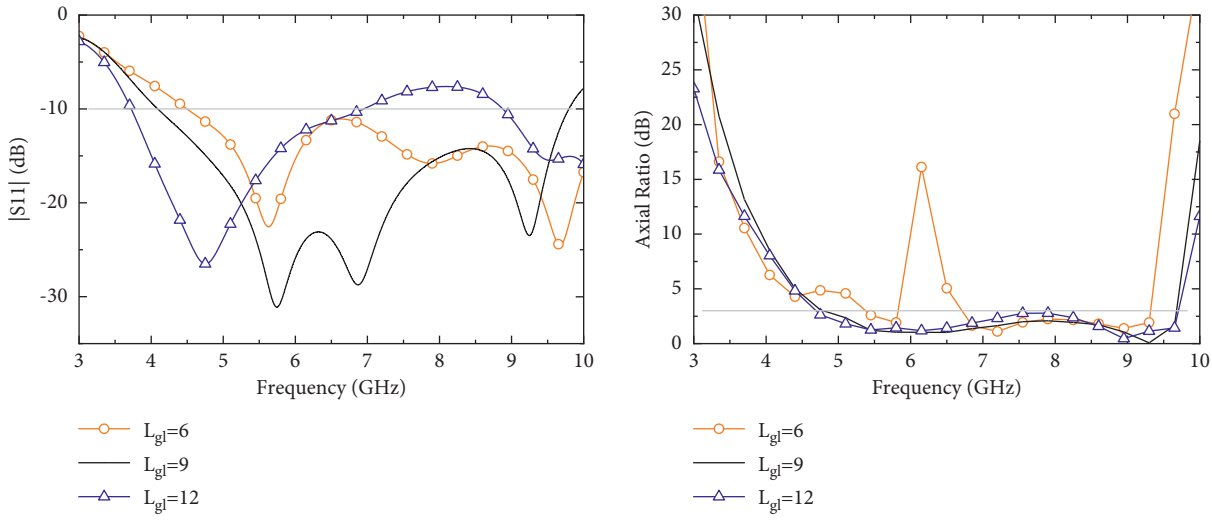

(b)

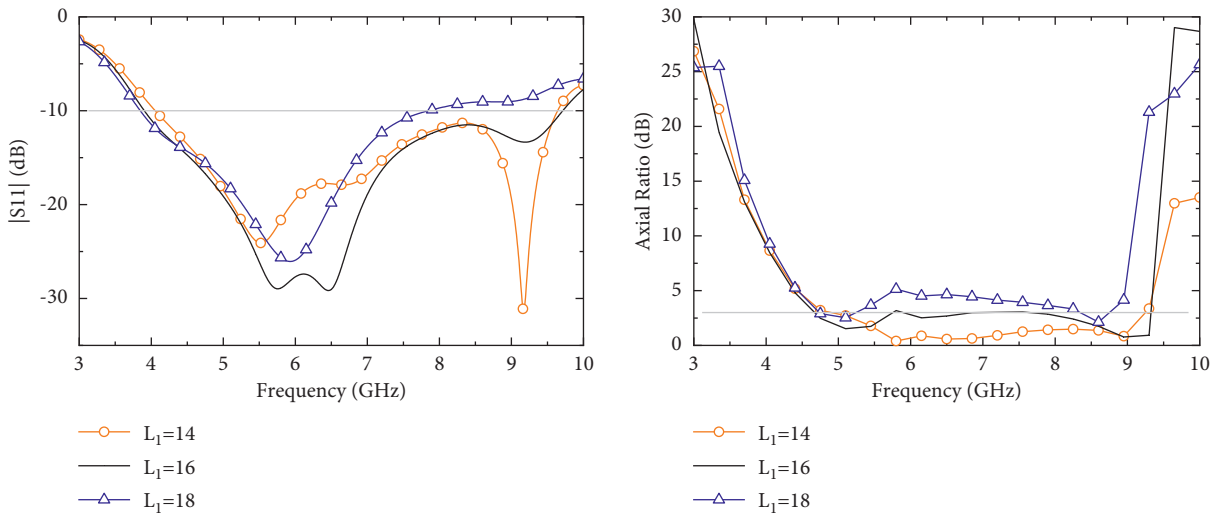

(c)

Figure 8: Continued.

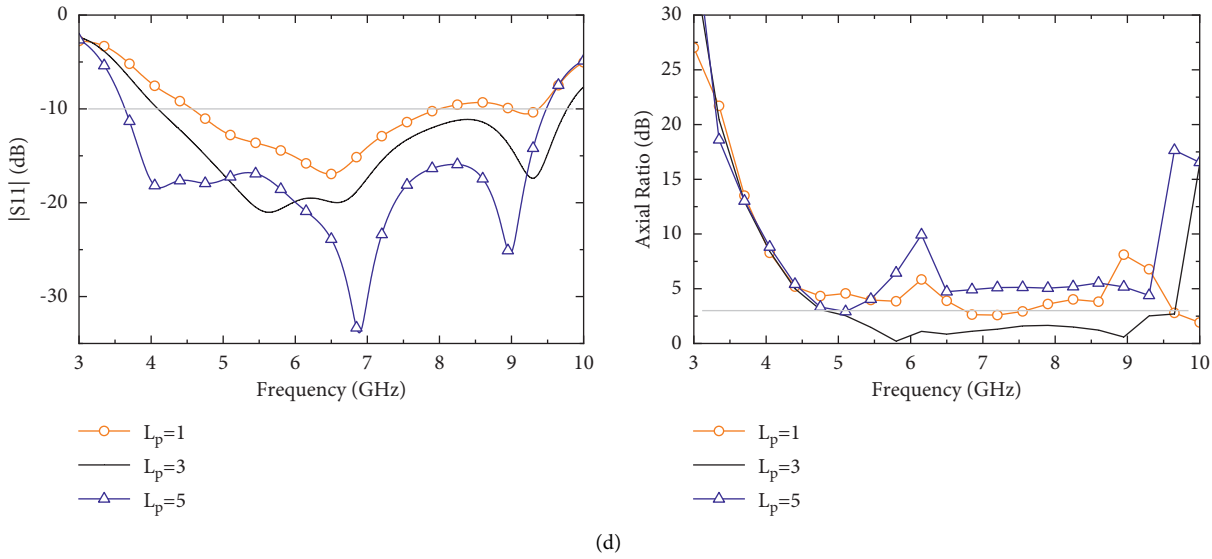

(d)

FIGURE 8: Simulated |S11| and AR of the proposed antenna for parametric analysis with different (a)W_g, (b) L_{gl}, (c) L_1, and (d) L_p.

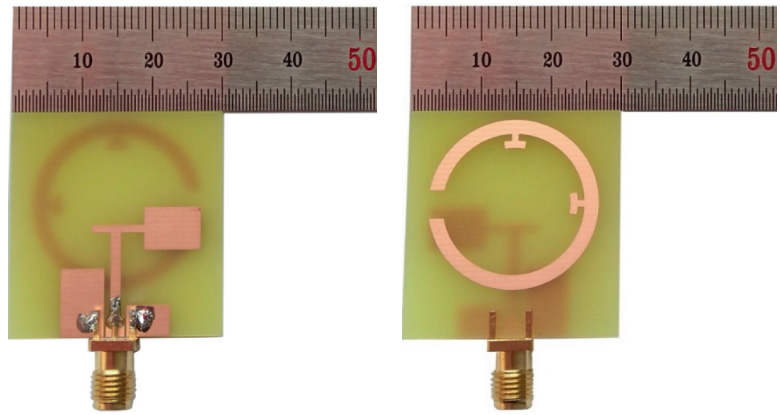

(a) (b)

FIGURE 9: Photographs of the fabricated antenna: (a) front view, (b) back view.

4. Experimental Verification

Figure 9 shows the photograph of the fabricated antenna and its measured and simulated S11, AR, and gain are curved in Figure 10. Measured and simulated results show good agreement, with slight discrepancies attributed to the fabrication tolerances and measure error. The measured 10-dB impedance bandwidth is 83.8% centered at 6.85 GHz (3.98–9.72 GHz), and the measured 3-dB AR bandwidth is 70.3% (4.59–9.57 GHz). Compared with the information provided by CMA, the introduction of the CPW feed causes the CP modes to move slightly toward higher frequencies. Additionally, a wider ARBW is obtained, which may be due to the feed moving high order modes to higher frequencies or introducing new modes to form CP modes contributing CP radiation over the upper band to broaden ARBW. It is found that the antenna gain has a maximum value of 3.1 dBic with a variation of less than 1.5 dB within the CP operation band.

Figure 11 depicts the measured radiation patterns in x-z and y-z planes at 5.5, 7.5, and 9.5 GHz, which is measured in the anechoic chamber with 8-meter distance between the antennas. It satisfies the far-field conditions of the proposed antenna and the standard antennas. It can be seen that the antenna radiates LHCP waves in the $+z$-direction. Furthermore, the opposite circular polarization at 5.5 GHz is realized for $z < 0$. However, the LHCP of $-z$ plane becomes high as the frequency increases, so that cross-polarization level deteriorates at 7.5 GHz and even the antenna radiates LHCP waves at 9.5 GHz with low gain. In other words, the antenna operated in a bidirectional manner with LHCP in the $+z$-direction and RHCP in the $-z$-direction at lower frequencies, and only LHCP is achieved over upper band.

Table 1 summarizes some key indicators of the proposed antenna and other wideband CP antennas. Apparently, there is a trade-off among lateral sizes, ARBW, and peak gain. The data indicates that the proposed antenna exhibits a

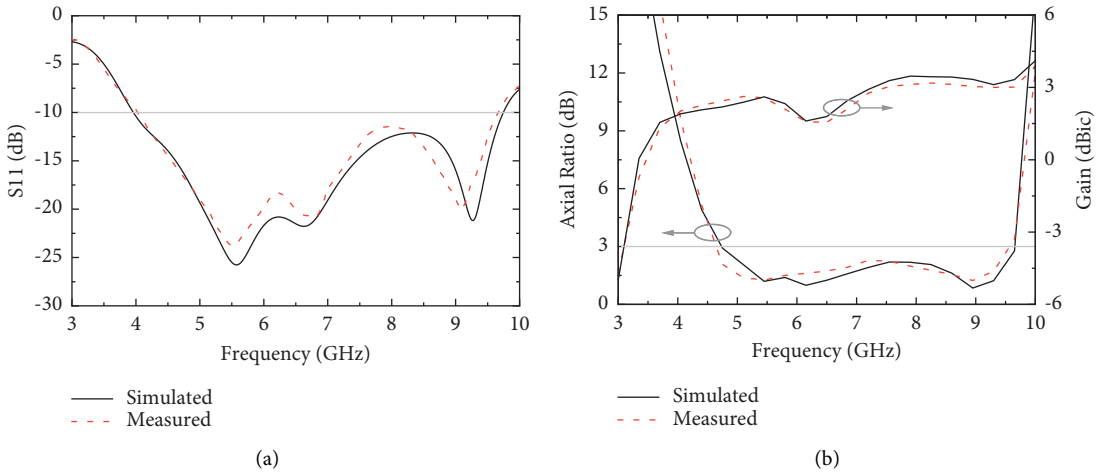

Figure 10: Simulated and measured (a) S11. (b) AR and gain.

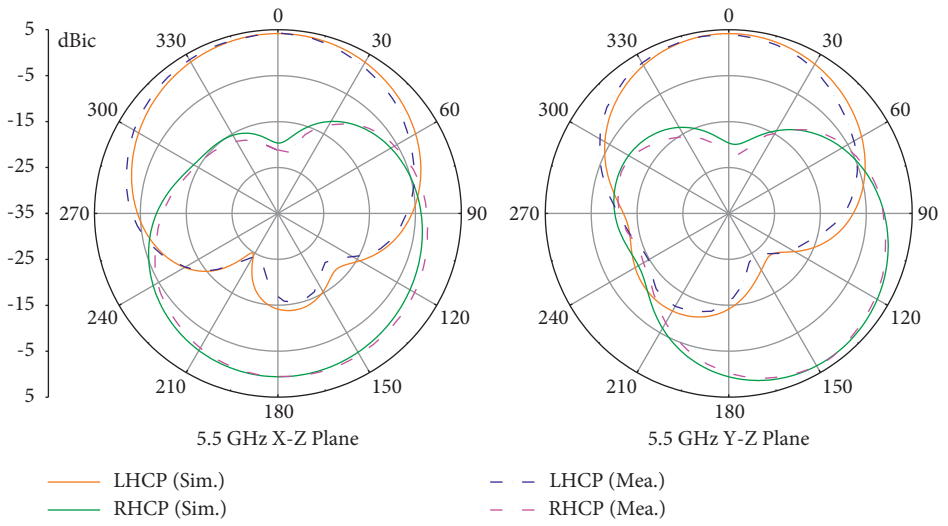

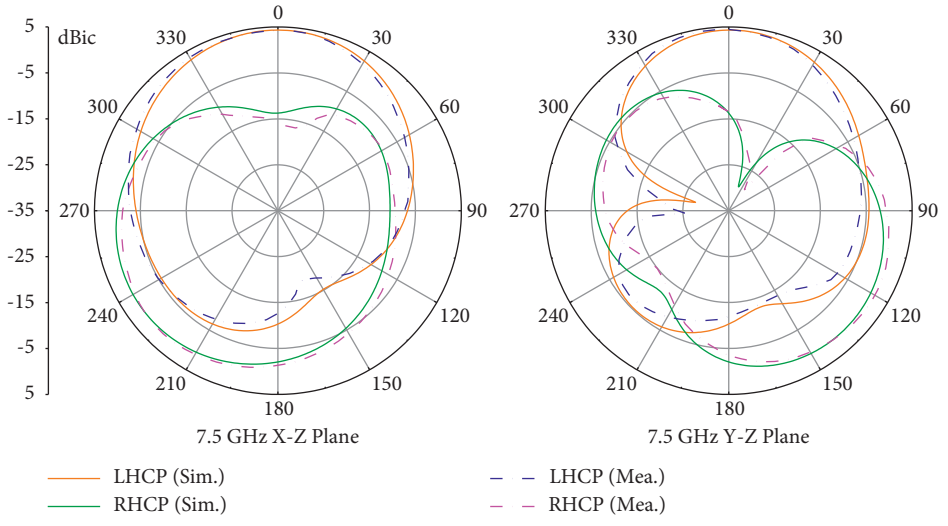

Figure 11: Continued.

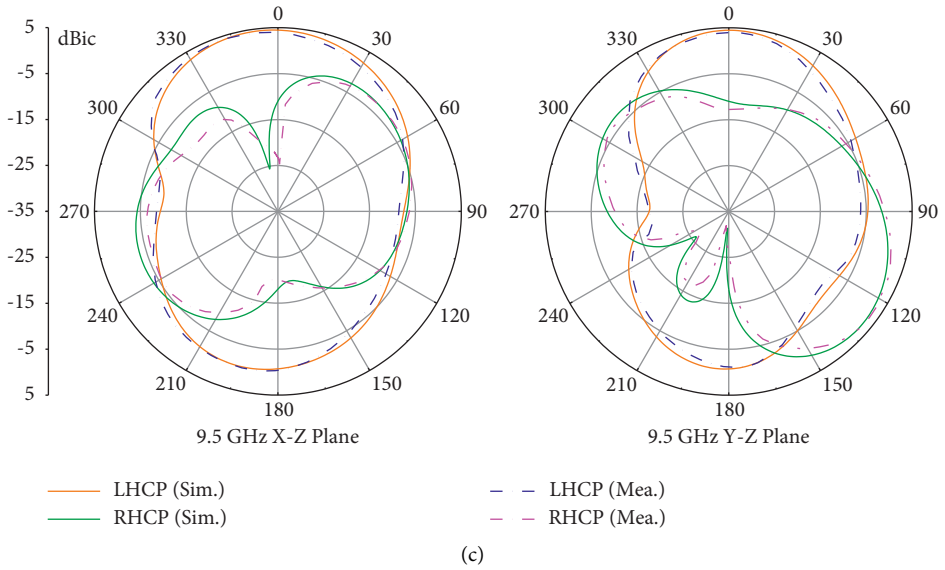

(c)

Figure 11: Simulated and measured radiation patterns at (a) 5.5 GHz, (b) 7.5 GHz, and (c) 9.5 GHz.

Table 1: Comparisons of the proposed and other CP antennas.

Ref.	Dimensions ($\lambda_0 \times \lambda_0 \times \lambda_0$)	Impedance bandwidth	3-dB AR bandwidth	Peak gain (dBic)
[3]	$0.77 \times 0.77 \times 0.008$	132.0% (0.85–4.15 GHz)	95.7% (1.20–3.40 GHz)	4.7
[4]	$0.48 \times 0.47 \times 0.009$	72.0% (2.26–4.85 GHz)	65.0% (2.44–4.85 GHz)	3.8
[8]	$0.71 \times 0.50 \times 0.009$	133.0% (1.22–5.97 GHz)	76.0% (2.00–4.47 GHz)	3.9
[21]	$0.54 \times 0.54 \times 0.019$	More than 100%	91.0% (2.10–5.60 GHz)	3.2
[22]	$1.4 \times 1.4 \times 0.057$	38.8% (4.42–6.55 GHz)	14.3% (5.20–6.00 GHz)	9.4
[26]	$0.36 \times 0.28 \times 0.017$	84.6% (2.35–5.8 GHz)	43.4% (2.40–3.73 GHz)	About 3.8
Prop.	$0.76 \times 0.71 \times 0.038$	83.8% (3.98–9.72 GHz)	70.3% (4.59–9.57 GHz)	3.1

Impedance bandwidth: $|S11| < 10$ dB, AR bandwidth: AR<3 dB, λ_0: free-space wavelength at the center frequency of the 3-dB AR bandwidth.

maximum absolute value of ARBW. The electrical size of the proposed antenna is in the middle of the reference antennas. The size comparisons are performed based on center frequency of the AR at the free-space wavelength (λ_0). Although the peak gain of the proposed antenna is smallest in all cases, it has better flatness over the CP operation band. Overall, the antenna shows a comparable performance in terms of dimension, impedance bandwidth, AR bandwidth, and process complexity.

5. Conclusion

The compact broadband circularly polarized antenna has been proposed based on characteristic mode analysis. Two arc-shaped metallic stubs and a gap have been introduced for the ring patch to generate CP radiation. Taking advantage of the orthogonality property of CMs, current distribution and radiation pattern of the CP modes have been investigated and then the CPW feeding structure with asymmetric ground planes has been designed and placed appropriately to excite the desired modes based on the information provided by CMA. Subsequently, the CPW-fed network is optimized by full-wave simulation for wideband impedance matching and AR. A prototype of the antenna has been fabricated. Experimental and simulated results with good agreement have been presented to validate the effectiveness of the design method with CMA, which paves the way for further development of CP antenna designs.

Data Availability

The data used to support the findings of this study are included within the article.

Conflicts of Interest

The authors declare that they have no conflicts of interest.

Acknowledgments

This work was supported by the National Natural Science Foundation of China General Program, under Grant 61971210 and Youth project of Liaoning Provincial Department of Education under Grant LJ2019QL024.

References

[1] C. A. Balanis, "Antenna theory: analysis and design," *IEEE Antennas and Propagation Society Newsletter*, vol. 24, no. 6, pp. 28-29, 2003.

[2] E. Arnieri, L. Boccia, G. Amendola, and G. Di Massa, "A compact high gain antenna for small satellite applications," *IEEE Transactions on Antennas and Propagation*, vol. 55, no. 2, pp. 277–282, 2007.

[3] X. Rui, J. Y. Li, and L. Jie, "A design of broadband circularly polarized c-shaped slot antenna with sword shaped radiator and its array for l/s-band applications," *IEEE Access*, vol. 99, p. 1, 2017.

[4] Ullah, Ubaid, Koziel, and Slawomir, "A novel coplanar- strip-based excitation technique for design of broadband circularly polarization antennas with wide 3 dB axial ratio beamwidth," *IEEE Transactions on Antennas and Propagation*, vol. 67, no. 7, 2019.

[5] Y.-X. Guo, K.-W. Khoo, and L. C. Ong, "Wideband circularly polarized patch antenna using broadband baluns," *IEEE Transactions on Antennas and Propagation*, vol. 56, no. 2, pp. 319–326, 2008.

[6] R. B. Waterhouse, "Stacked patches using high and low di-electric constant material combinations," *IEEE Transactions on Antennas and Propagation*, vol. 47, no. 12, pp. 1767–1771, 1999.

[7] R. K. Saini, S. Dwari, and M. K. Mandal, "Cpw-fed dual- band dual-sense circularly polarized monopole antenna," *IEEE Antennas and Wireless Propagation Letters*, vol. 81, p. 1, 2017.

[8] C.-J. Wang and W.-B. Tsai, "Microstrip open-slot antenna with broadband circular polarization and impedance bandwidth," *IEEE Transactions on Antennas and Propagation*, vol. 64, no. 9, pp. 4095–4098, 2016.

[9] C.-J. Wang, M.-H. Shih, and L.-T. Chen, "A wideband open-slot antenna with dual-band circular polarization," *IEEE Antennas and Wireless Propagation Letters*, vol. 14, pp. 1306–1309, 2015.

[10] J. Wu, Y. J. Cheng, and Y. Fan, "Millimeter-wave wide- band high-efficiency circularly polarized planar array antenna," *IEEE Transactions on Antennas and Propagation*, vol. 64, no. 2, p. 1, 2016.

[11] E. E. Altshuler, "Design of a vehicular antenna for gps/iridium using a genetic algorithm," *IEEE Transactions on Antennas and Propagation*, vol. 48, no. 6, pp. 968–972, 2000.

[12] R. L. Haupt, "Antenna design with a mixed integer genetic algorithm," *IEEE Transactions on Antennas and Propagation*, vol. 55, no. 3, pp. 577–582, 2007.

[13] Y. Chen and C. F. Wang, *Characteristic Modes: Theory and Applications in Antenna Engineering*, Wiley, Hoboken, NJ, USA, 2015.

[14] W. Li, Y. Liu, J. Li, L. Ye, and Q. H. Liu, "Modal proportion analysis in antenna characteristic mode theory," *International Journal of Antennas and Propagation*, vol. 2019, Article ID 7069230, 10 pages, 2019.

[15] E. Antonino-Daviu, M. Fabres, M. Ferrando-Bataller, and V. M. R. Penarrocha, "Modal analysis and design of band-notched UWB planar monopole antennas," *IEEE Transactions on Antennas and Propagation*, vol. 58, no. 5, pp. 1457–1467, 2010.

[16] E. Antonino-Daviu, M. Cabedo-Fabrés, M. Sonkki, N. M. Mohamed-Hicho, and M. Ferrando-Bataller, "Design guidelines for the excitation of characteristic modes in slotted planar structures," *IEEE Transactions on Antennas and Propagation*, vol. 64, no. 12, p. 1, 2016.

[17] F. H. Lin and Z. N. Chen, "Low-profile wide- band metasurface antennas using characteristic mode analysis," *IEEE Transactions on Antennas and Propagation*, vol. 65, 2017.

[18] R. Martens, E. Safin, and D. Manteuffel, "Inductive and capacitive excitation of the characteristic modes of small terminals," in *Proceedings of the Antennas and Propagation Conference*, Rome, Italy, April 2011.

[19] P. W. Futter and U. Jakobus, "Antenna positioning for bandwidth optimization using characteristic mode analysis," in *Proceedings of the 2020 14th European Conference on Antennas and Propagation (EuCAP)*, Copenhagen, Denmark, March 2020.

[20] Y. Chao-Fu Wang and C. F. Wang, "Characteristic-mode-based improvement of circularly polarized u-slot and e-shaped patch antennas," *IEEE Antennas and Wireless Propagation Letters*, vol. 11, pp. 1474–1477, 2012.

[21] H. H. Tran, N. Nguyen-Trong, and A. M. Abbosh, "Sim- ple design procedure of a broadband circularly polarized slot monopole antenna assisted by characteristic mode analysis," *IEEE Access*, vol. 99, p. 1, 2018.

[22] C. Zhao and C. F. Wang, "Characteristic mode design of wide band circularly polarized patch antenna consisting of h-shaped unit cells," *IEEE Access*, vol. 99, p. 1, 2018.

[23] L. Chang, L.-L. Chen, J.-Q. Zhang, and D. Li, "A wideband circularly polarized antenna with characteristic mode analysis," *International Journal of Antennas and Propagation*, vol. 2020, Article ID 5379892, 13 pages, 2020.

[24] J. F. Lin and L. Zhu, "Low-profile high-directivity circularly-polarized differential-fed patch antenna with characteristic modes analysis," *IEEE Transactions on Antennas and Propagation*, vol. 99, p. 1, 2020.

[25] R. Harrington and J. Mautz, "Theory of characteristic modes for conducting bodies," *IEEE Transactions on Antennas and Propagation*, vol. 19, 1971.

[26] M. Han and W. Dou, "Compact clock-shaped broadband circularly polarized antenna based on characteristic mode analysis," *IEEE Access*, vol. 99, p. 1, 2019.